REFERENCES AND NOTES

1. S. Luyssaert *et al.*, *Glob. Change Biol.* **16**, 1429–1450 (2010).
2. B. Schlamadinger, G. Marland, *Biomass Bioenergy* **10**, 275–300 (1996).
3. T. W. Hudiburg, B. E. Law, C. Wirth, S. Luyssaert, *Nat. Clim. Change* **1**, 419–423 (2011).
4. UN, *Kyoto Protocol to the United Nations Framework Convention on Climate Change* (1998); http://unfccc.int/kyoto_protocol/items/2830.php.
5. B. Amiro *et al.*, *Agric. For. Meteorol.* **136**, 237–251 (2006).
6. J.-Y. Juang, G. Katul, M. Siqueira, P. Stoy, K. Novick, *Geophys. Res. Lett.* **34**, L21408 (2007).
7. E. Rotenberg, D. Yakir, *Science* **327**, 451–454 (2010).
8. S. Luyssaert *et al.*, *Nat. Clim. Change* **4**, 389–393 (2014).
9. R. A. Pielke Sr. *et al.*, *Philos. Trans. A Math. Phys. Eng. Sci.* **360**, 1705–1719 (2002).
10. R. A. Pielke *et al.*, *WIREs Clim. Change* **2**, 828 (2011).
11. A. J. Pitman *et al.*, *Geophys. Res. Lett.* **36**, L14814 (2009).
12. J. Pongratz, T. Raddatz, C. H. Reick, M. Esch, M. Claussen, *Geophys. Res. Lett.* **36**, GB3018 (2009).
13. R. Mahmood *et al.*, *Int. J. Climatol.* **34**, 929–953 (2014).
14. M. J. McGrath *et al.*, *Biogeosciences* **12**, 4291–4316 (2015).
15. Materials and methods are available as supplementary materials on *Science* Online.
16. K. Naudts *et al.*, *Geosci. Model Dev.* **8**, 2035–2065 (2015).
17. P. Meyfroidt, E. F. Lambin, *Annu. Rev. Environ. Resour.* **36**, 343–371 (2011).
18. M. Bürgi, A. Schuler, *For. Ecol. Manage.* **176**, 173–183 (2003).
19. E. P. Farrell *et al.*, *For. Ecol. Manage.* **132**, 5–20 (2000).
20. K. Klein Goldewijk, A. Beusen, P. Janssen, *Holocene* **20**, 565–573 (2010).
21. U. Gimmi, M. Bürgi, M. Stuber, *Ecosystems* **11**, 113–124 (2008).
22. X. Lee *et al.*, *Nature* **479**, 384–387 (2011).
23. Y. Li *et al.*, *Nat. Commun.* **6**, 6603 (2015).
24. M. Zhang *et al.*, *Environ. Res. Lett.* **9**, 034002 (2014).
25. W. Brutsaert, *Water Resour. Res.* **11**, 742–744 (1975).
26. J. Otto *et al.*, *Biogeosciences* **11**, 2411–2427 (2014).
27. Food and Agriculture Organization of the United Nations (FAO), *Global Forest Resources Assessment 2005. Progress Towards Sustainable Forest Management* (FAO Forestry Paper 147, FAO, 2006).

ACKNOWLEDGMENTS

K.N., J.R., Y.C., M.J.M., J.O., and S.L. were funded through European Research Council starting grant 242564 [DOFOCO (Do Forests Cool the Earth) program]. A.V. was funded through the French Environment and Energy Management Agency (ADEME, Bilan Carbone de la Forêt Française program). K.N. received additional funding through the Essential Climate Variables land cover program and the German Research Foundation's Emmy Noether Program (grant PO 1751/1-1). The study benefited from a Short-Term Scientific Mission [COST (European Cooperation in Science and Technology) TERRABITES (Terrestrial Biosphere in the Earth System) grant ES805] offered to K.N. Precipitation data from the Global Precipitation Climatology Centre were made available by the National Oceanic and Atmospheric Administration's Earth System Research Laboratory (Physical Science Division), Boulder, CO (www.esrl.noaa.gov/psd/). The ORCHIDEE and LMDZ project teams as well as the Centre de Calcul Recherche et Technologie provided the run environment that is essential for the type of coupled land-atmosphere simulations that were conducted in this study. The code and the run environment are open source and distributed under the CeCILL (CEA CNRS INRIA Logiciel Libre) license (http://labex.ipsl.fr/orchidee/). M.J.M., J.O., J.R., Y.C., K.N., A.V., and S.L designed the study and/or contributed to the interpretation of the results. M.J.M., J.O., J.R., Y.C., K.N., A.V., and S.L. developed, parameterized, and validated ORCHIDEE-CAN. M.J.M., Y.C., and S.L. conducted the simulation experiment. K.N., Y.C., M.J.M, J.O., S.L., and J.R. analyzed the data.

SUPPLEMENTARY MATERIALS

www.sciencemag.org/content/351/6273/597/suppl/DC1
Materials and Methods
Figs. S1 to S6
Tables S1 to S3
References (*28*–*75*)

26 October 2015; accepted 8 January 2016
10.1126/science.aad7270

CLIMATE CHANGE

Biophysical climate impacts of recent changes in global forest cover

Ramdane Alkama and Alessandro Cescatti*

Changes in forest cover affect the local climate by modulating the land-atmosphere fluxes of energy and water. The magnitude of this biophysical effect is still debated in the scientific community and currently ignored in climate treaties. Here we present an observation-driven assessment of the climate impacts of recent forest losses and gains, based on Earth observations of global forest cover and land surface temperatures. Our results show that forest losses amplify the diurnal temperature variation and increase the mean and maximum air temperature, with the largest signal in arid zones, followed by temperate, tropical, and boreal zones. In the decade 2003–2012, variations of forest cover generated a mean biophysical warming on land corresponding to about 18% of the global biogeochemical signal due to CO_2 emission from land-use change.

Forests play a relevant role in the climate system by absorbing approximately one-fourth of anthropogenic CO_2 emissions (*1*), storing large carbon pools in tree biomass and forest soils (*2*), and modulating the land-atmosphere exchange of energy and water vapor (*3*). Given the important role of forests in the global carbon cycle, climate treaties account for land-based mitigation options such as afforestation, reforestation, and avoided deforestation or forest degradation (*4*, *5*). On the contrary, the climate impacts of biophysical processes, such as the surface exchange of energy and water vapor (*6*), are still uncertain in sign and magnitude and therefore have not been considered in climate negotiations to date.

Over the past two decades, the biophysical effects of deforestation on climate have been assessed mainly by comparing paired model simulations with contrasting forest cover (*7*–*12*). These analyses have shown that, despite the increase in surface albedo, the net biophysical effects of tropical deforestation may increase surface temperature through the reduction of evapotranspiration (*9*, *13*). On the contrary, boreal deforestation may lead to net climate cooling due to the high snow albedo in cleared areas during winter/spring and to the land-albedo/sea-temperature feedback (*11*, *12*, *14*). However, results of these numerical experiments are model-dependent, and the uncertainties in sign, magnitude, and spatial distribution of the predicted effects are very large (*15*–*17*). Therefore, direct observations of the biophysical climate effects of recent forest losses and gains are required to constrain predictions, reduce the uncertainty of model ensembles, and provide robust recommendations to climate policy.

To date, data-driven assessments based on in situ (*18*–*20*) or satellite observations (*3*, *21*, *22*) have adopted the space-for-time analogy, meaning that spatial differences in surface temperature between areas with contrasting forest cover have been interpreted as the climate signal of hypothetical deforestation/afforestation. The substitution of space for time produces unbiased results only if forests are randomly distributed in the landscape. Conversely, the systematic location of forests in less favorable areas (such as steeper or colder slopes, shallow soils, etc.) may produce spatial gradients in surface climate that should not be attributed to changes in land cover (*18*). In addition, both model-based and observation-based assessments have focused so far on idealized scenarios of deforestation (*10*, *11*) and on the estimation of climate sensitivities to land-use change (*3*, *18*, *22*), but the climate signal generated by the ongoing changes in forest cover has not yet been quantified.

To overcome the limits and uncertainties of past assessments, in this work we focused on areas that underwent recent land cover transitions, with the objective of providing a global, robust, and data-driven assessment of the biophysical climate impacts of observed forest gains and losses. The analysis builds on overlapping satellite retrievals of surface radiometric temperature (*23*) and of high-resolution variations in forest cover (*24*). A novel methodology has been developed to disentangle the effect of forest cover change from the global climate signal [details in supplementary materials (SM) text S1.2]. For this purpose, the temperature difference (ΔT) between two years at a given location is expressed as the effect of forest cover change (ΔT_{fcc}) plus the residual signal (ΔT_{res}) due to climate variability (Eq. 1)

$$\Delta T = \Delta T_{fcc} + \Delta T_{res} \rightarrow \Delta T_{fcc} = \Delta T - \Delta T_{res} \quad (1)$$

The temporal variation in air surface temperature (ΔT) is estimated from satellite retrievals of radiometric land surface temperature, evapotranspiration, and albedo, with semi-empirical models calibrated against in situ measurements of air temperature (SM text S1.1 and figs. S1 and S2). For a given location, we derive ΔT_{fcc} from Eq. 1 by estimating ΔT_{res} from adjacent areas with stable forest cover and therefore where $\Delta T_{fcc} \simeq 0$

European Commission, Joint Research Centre, Institute for Environment and Sustainability, Ispra, Italy.
***Corresponding author. E-mail: alessandro.cescatti@jrc.ec.europa.eu**

and $\Delta T \simeq \Delta T_{res}$ (fig. S4). To estimate ΔT_{res}, areas located within 50 km of the target location were considered, using the inverse distance as a weighting factor (methods in SM text S1.2). At a seasonal time scale, the residual signal ΔT_{res} is typically in the range ±1.5°C, as the temperature signal of forest cover changes (fig. S4). We focused the analysis on the first and last year of the available time series (i.e., 2003 and 2012) in order to maximize the observed land cover change and therefore the spatial extent and robustness of the estimates. In parallel, the interannual variability of the climate signal was investigated by comparing 2003 with each of the other years, and the robustness of the signal was estimated on an ensemble of nine pairs of years (2003–2005 versus 2010–2012; methods in SM text S1.2.2).

Results show that in all climate zones, forest clearing produces a marked increase of mean annual maximum air surface temperatures, slight changes in minimum temperatures, and an overall increase of mean temperatures, except at the northernmost latitudes (Fig. 1, B and C). In fact, the removal of forest cover does not significantly affect the mean air temperature in the boreal zone, whereas it increases the temperature by about 1°C in the temperate and tropical zones and by more than 2°C in the arid zone (Fig. 1C). These signals show limited interannual variability and a decreasing uncertainty at the increase of the time interval and therefore of the area affected by cover change (fig. S9). In the temperate and boreal zones, the warming induced by forest losses declines over time, presumably because of the progressive recovery of vegetation in forest clearings. On the contrary, tropical areas show a stable signal, likely due to the conversion of forests to agriculture (fig. S9).

The methodology used in Fig. 1 to investigate mean annual temperatures has been replicated at a monthly time scale to explore the seasonal temperature sensitivity (Fig. 2 and figs. S5 and S6). These monthly signals show a limited variability between years in the different climate zones and latitudinal bands (figs. S10 and S11). The climate impact of deforestation is modulated by the incoming radiation and, as a consequence, the largest warming occurs during the summer solstice at maximum temperatures, whereas changes in air temperatures during nighttime are negligible. The substantial reduction of evapotranspiration

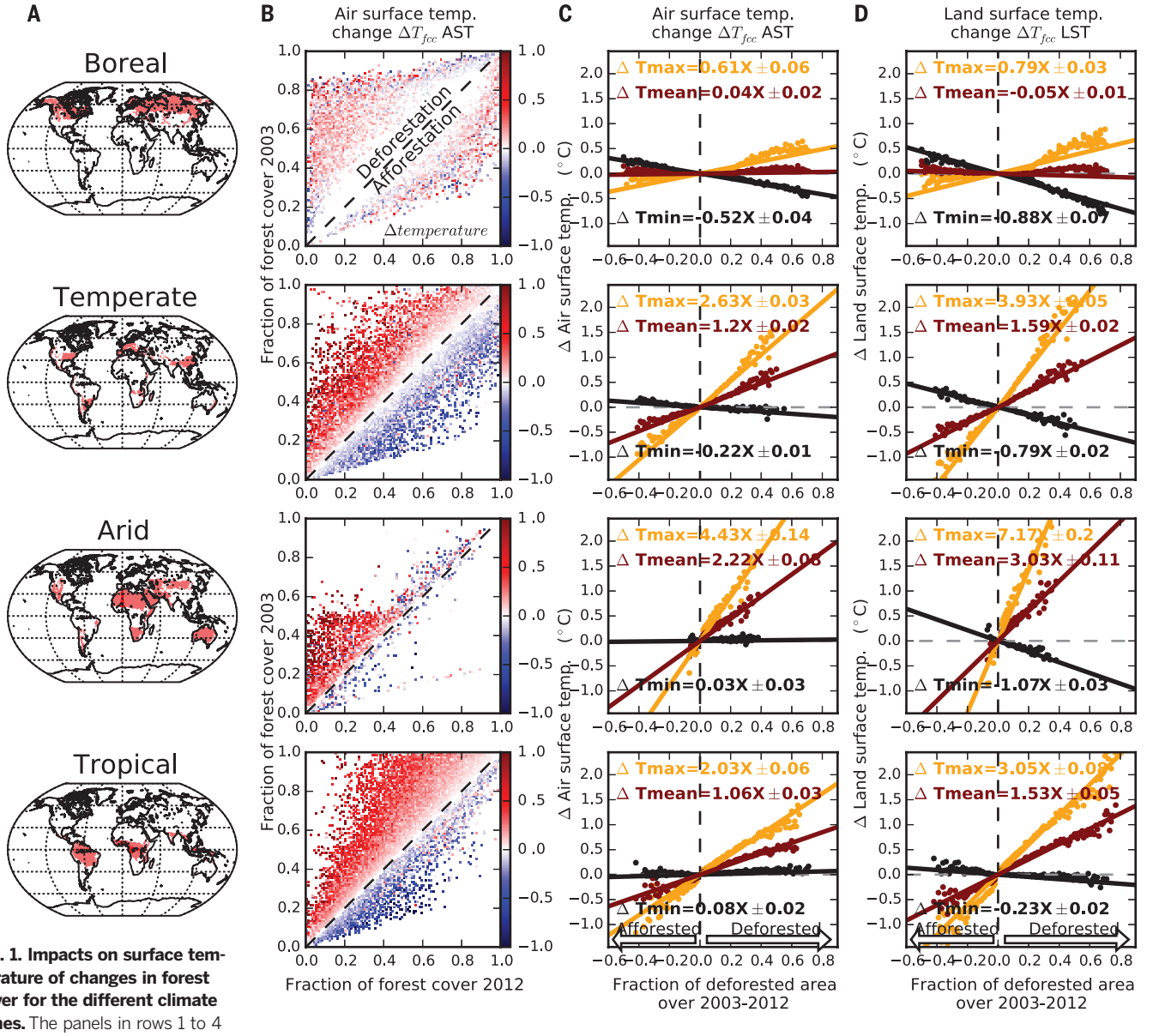

Fig. 1. Impacts on surface temperature of changes in forest cover for the different climate zones. The panels in rows 1 to 4 show the observed climate impacts of changes in forest cover between 2003 and 2012 in the climate zones defined in (**A**). (**B**) Observed variations in mean annual air surface temperature due to observed changes in forest cover (seasonal plots are reported in figs. S5 and S6). The sensitivity of the mean (dark red), minimum (black), and maximum (orange) air surface temperatures (**C**) and land surface temperature (**D**) to the fraction of the deforested area is shown.

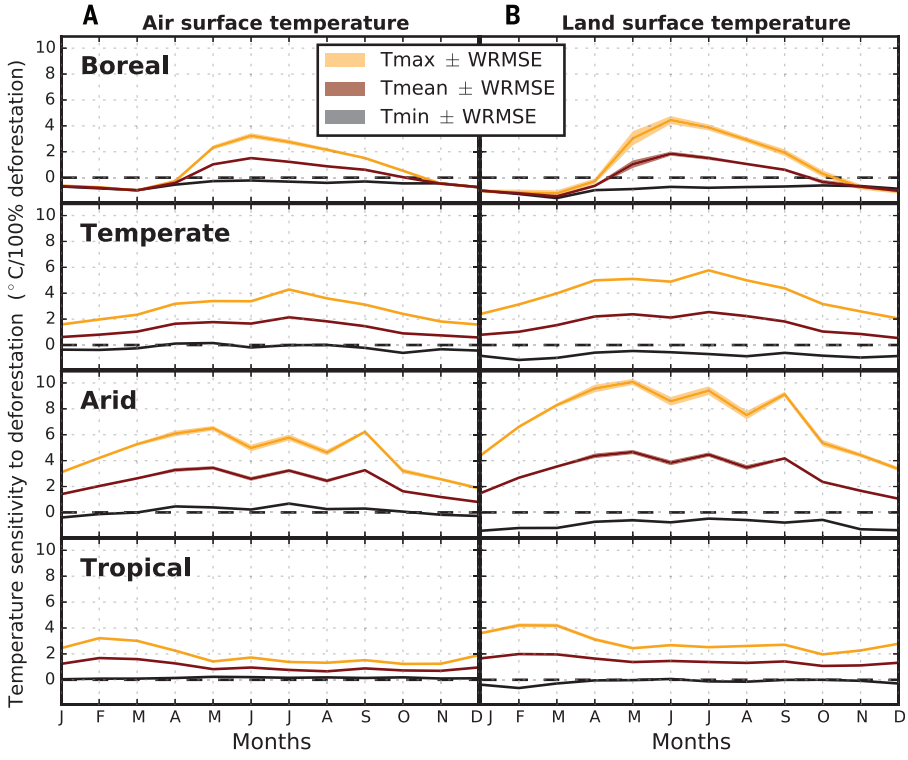

Fig. 2. Seasonal changes in air and land surface temperature due to losses of forest cover. Expected changes in the monthly maximum, minimum, and mean air (**A**) and land (**B**) surface temperature due to the total clearing of a 0.05° grid cell in the different climate zones are shown (mean ± weighted root mean square error, WRMSE).

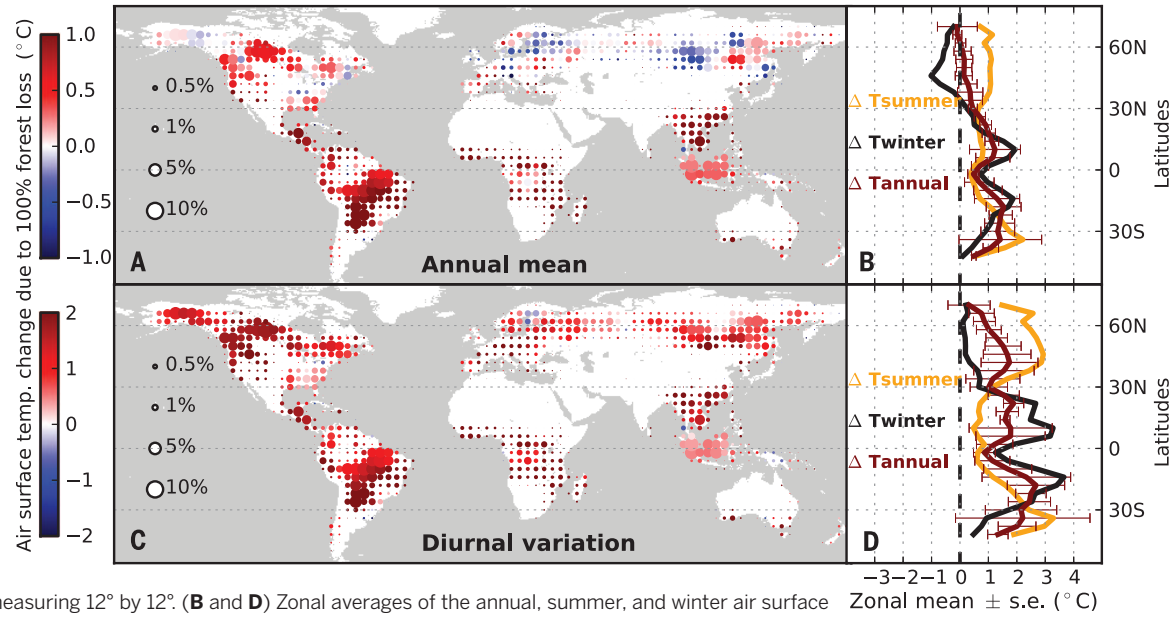

Fig. 3. Regional changes in air surface temperature due to losses in forest cover between 2003 and 2012. Changes in mean annual air temperature (**A**) and diurnal variations (**C**) due to forest losses are shown. The symbol size indicates the magnitude of forest cover losses, and the color specifies the average temperature sensitivity to total deforestation. Points are spaced 4° in both latitude and longitude, and statistics were computed in windows measuring 12° by 12°. (**B** and **D**) Zonal averages of the annual, summer, and winter air surface temperature statistics at 4° of latitudinal resolution (the equivalent image for land surface temperature is reported in fig. S7).

and surface roughness with forest clearing (*11*, *13*) is the most plausible explanation for the substantial local warming under high radiation load. The remarkable daytime warming ultimately leads to an increase in the diurnal variation (the difference between the daily maximum and minimum temperature) of about 1.13 ± 0.1°C, 2.85 ± 0.04°C, 4.4 ± 0.17°C, and 1.95 ± 0.08°C over the boreal, temperate, arid, and tropical climate zones, respectively. In summary, forests show important biophysical mitigation effects on local maximum temperature in all climate zones, by reducing local daytime summer temperatures and substantially decreasing the diurnal and annual temperature variations. The key role of evapotranspiration in the biophysical impacts of forest clearing emerges from the ranking of the climate zones, with the arid areas showing the strongest signal, followed by the temperate, the tropical, and the boreal zones.

Climate sensitivity to losses of forest cover was investigated at the regional scale by applying in a 12°-by-12° moving window the same methodology used to investigate the climate zones (Fig. 3 and fig. S7; methods in SM text S1.2.1). This analysis shows that forest losses in tropical areas generate warming across all seasons. Contrasting effects occur at northern latitudes between seasons (winter cooling and summer warming) and continents (warming in North America and cooling in

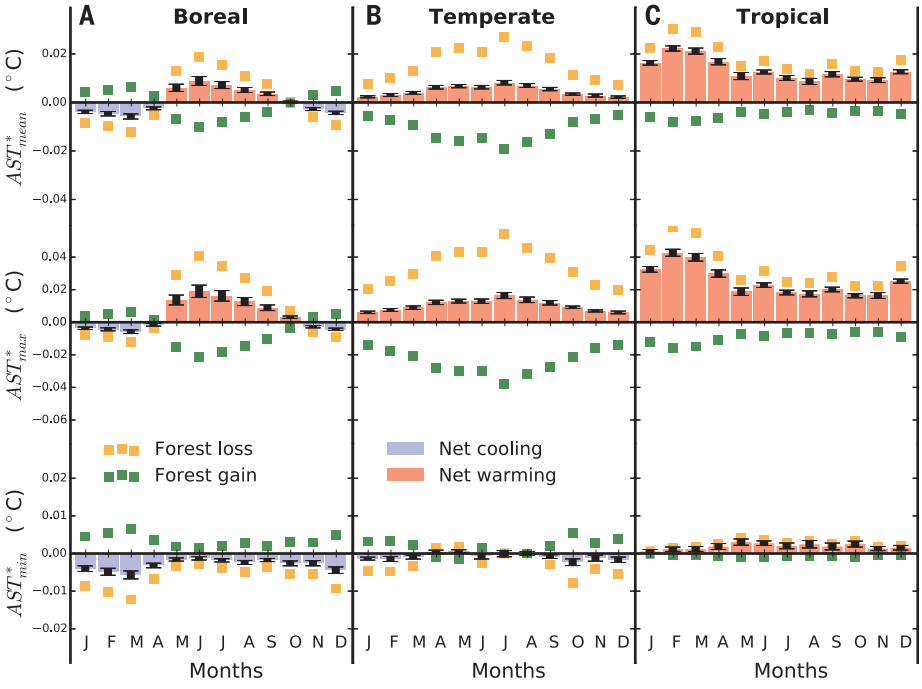

Fig. 4. Net impact of deforestation and afforestation on monthly air surface temperatures. Changes in monthly mean, maximum, and minimum air surface temperature due to forest cover change over the (**A**) boreal, (**B**) temperate, and (**C**) tropical climate zones (the arid zone has experienced minor changes in forest cover) are shown. Yellow and green squares represent the global temperature signal of forest cover losses and gains, and light red and blue bars indicate the warming and cooling due to the net change in forest cover (the equivalent image for land surface temperature is shown in fig. S8).

northern Eurasia, Fig. 3, A and B). In accordance with observations performed in North America (*18*, *20*), forest clearing increases the diurnal temperature variation during summer months at all latitudes (Fig. 3, C and D), whereas it has no effects on the diurnal variation during the boreal winter, because of the dominant effect of snow albedo. The changes in diurnal temperature variation (Fig. 3D) are substantially larger than those in mean annual temperature (Fig. 3B). These results highlight the fact that local biophysical processes triggered by forest losses can effectively increase summer temperatures in all world regions, further amplifying the climate trends driven by the increasing greenhouse gas concentrations.

The estimated rate of local warming after forest losses is lower than that predicted by observation-driven studies focused on land surface temperature (*22*). In addition, the low sensitivity of the mean annual temperature observed at northern latitudes is in contrast with model simulations of large-scale deforestation that typically predict a sharp reduction in boreal temperatures (*8*, *10*), possibly amplified by land-ocean interactions (*11*). Differently from previous assessments (*3*, *22*), our analysis focused on air surface temperature instead of land surface temperature, given the greater relevance of the first parameter in climate science. On this aspect Figs. 1, C and D, and 2 show that the sensitivity of land surface temperature to changes in forest cover is about 50% larger than that of air temperature. This large difference is probably driven by satellite retrievals of land surface temperature that are biased toward clear sky conditions, when the biophysical differences between land covers are maximized. In addition, it is important to consider that our analysis quantifies the local impacts of fine-scale variations in forest cover that are primarily driven by changes in the surface energy budget and related first-order interactions with the boundary layer. Therefore, this assessment cannot capture the signal of large-scale land-atmosphere interactions and regional teleconnections. On the contrary, model experiments of idealized large-scale deforestation also account for second-order effects and feedbacks (such as changes in cloud cover, rainfall, sea surface temperature, etc.) that may amplify and eventually override the local temperature signal of deforestation (*25*). In particular, significant feedbacks between land surface albedo and sea temperature seem to drive the temperate/boreal cooling in model experiments of global deforestation (*11*).

Afforestation or reforestation can significantly attenuate the biophysical effect of forest clearing on surface temperature, especially over boreal and temperate zones, where gains in forest cover compensated for more than 60% of forest losses in the decade 2003–2012 (Fig. 4A). On the contrary, over the same period, forest gains offset less than 30% of the losses in the tropics, leading to a significant net deforestation (*24*, *26*) (Fig. 4C). The strong local effect of the changes in forest cover on air surface temperature turns out to be rather minor when averaged over the year at the global scale (0.0062°C, Fig. 4), due to the attenuation effect of the boreal winter and of nighttime temperatures, to the compensatory effect of forest gains, and to the limited extent of forest losses. On average, in the analyzed decade, the global biophysical warming due to changes in forest cover is equal to about 18% (12 to 42%) of the biogeochemical warming due to CO_2 emissions from land-use change (methods in SM text S1.3).

This analysis reveals that the biophysical effects of changes in forest cover can substantially affect the local climate by altering the average temperature and, even more markedly, the maximum summer temperatures and the diurnal and annual variations (*18*, *20*). In addition to the global mitigation effects of the terrestrial carbon sink (*1*), the biophysical properties of forests can therefore contribute to the mitigation of climate extremes, in particular by reducing daytime temperatures during summer months (*27*). These effects are relevant both in the tropics, where deforestation rates are still substantial and forest clearing generates warming throughout the whole year, and in the boreal zone, where forests contribute to the mitigation of rapidly increasing summer temperatures. Overall, the observation-driven global quantification of the biophysical signal of deforestation provided in this study may support accounting for land biophysics in climate negotiations, as well as the definition of novel protocols for the measurement, reporting, and verification of these relevant effects.

REFERENCES AND NOTES

1. C. Le Quéré *et al.*, *Earth Syst. Sci. Data.* **6**, 235–263 (2014).
2. N. Carvalhais *et al.*, *Nature* **514**, 213–217 (2014).
3. K. Zhao, R. B. Jackson, *Ecol. Monogr.* **84**, 329–353 (2014).
4. D. E. Schulze, C. Wirth, M. Heimann, *Science* **289**, 2058–2059 (2000).
5. H. K. Gibbs, S. Brown, J. O. Niles, J. A. Foley, *Environ. Res. Lett.* **2**, 045023 (2007).
6. G. B. Bonan, *Science* **320**, 1444–1449 (2008).
7. J. Lean, D. Warrilow, *Nature* **342**, 411–413 (1989).
8. P. K. Snyder, C. Delire, J. Foley, *Clim. Dyn.* **23**, 279–302 (2004).
9. J. J. Feddema *et al.*, *Science* **310**, 1674–1678 (2005).
10. G. Bala *et al.*, *Proc. Natl. Acad. Sci. U.S.A.* **104**, 6550–6555 (2007).
11. E. L. Davin, N. de Noblet-Ducoudre, *J. Clim.* **23**, 97–112 (2010).
12. N. de Noblet-Ducoudré *et al.*, *J. Clim.* **25**, 3261–3281 (2012).
13. G. A. Ban-Weiss, G. Bala, L. Cao, J. Pongratz, K. Caldeira, *Environ. Res. Lett.* **6**, 034032 (2011).

14. M. M. Loranty, L. T. Berner, S. J. Goetz, Y. Jin, J. T. Randerson, *Glob. Change Biol.* **20**, 594–606 (2014).
15. A. J. Pitman *et al.*, *Geophys. Res. Lett.* **36**, L14814 (2009).
16. V. Brovkin *et al.*, *J. Adv. Model. Earth Syst.* **5**, 48–57 (2013).
17. L. R. Boysen *et al.*, *Earth Syst. Dyn. Discuss.* **5**, 443–472 (2014).
18. X. Lee *et al.*, *Nature* **479**, 384–387 (2011).
19. S. Luyssaert *et al.*, *Nat. Clim. Change* **4**, 389–393 (2014).
20. M. Zhang *et al.*, *Environ. Res. Lett.* **9**, 034002 (2014).
21. S.-S. Peng *et al.*, *Proc. Natl. Acad. Sci. U.S.A.* **111**, 2915–2919 (2014).
22. Y. Li *et al.*, *Nat. Commun.* **6**, 6603 (2015).
23. Z. Wan, *Remote Sens. Environ.* **140**, 36–45 (2014).
24. M. C. Hansen *et al.*, *Science* **342**, 850–853 (2013).
25. P. K. Snyder, *Earth Interact.* **14**, 1–34 (2010).
26. F. Achard *et al.*, *Glob. Change Biol.* **20**, 2540–2554 (2014).
27. A. J. Teuling *et al.*, *Nat. Geosci.* **3**, 722–727 (2010).

ACKNOWLEDGMENTS

The authors gratefully acknowledge G. Duveiller and F. Achard for inspiring discussions and valuable inputs. The authors acknowledge the use of forest cover data from the University of Maryland (http://earthenginepartners.appspot.com/science-2013-global-forest); gridded air surface temperature data TS.3.22 from the Climatic Research Unit, University of East Anglia (http://catalogue.ceda.ac.uk/uuid/3f8944800cc48e1cbc29a5ee12d8542d); and in situ monthly data of air temperature from the Global Historical Climatology Network (GHCN-Monthly, http://www.ncdc.noaa.gov/ghcnm/v3.php) of the National Oceanic and Atmospheric Administration's National Climatic Data Center. The MODIS products LST MYD11C3 and NDVI MYD13C2 were retrieved through the online data pool of the NASA Land Processes Distributed Active Archive Center (https://lpdaac.usgs.gov). The authors are grateful to C. Martinez for the linguistic revision. The work was supported by the European Commission JRC-IES-H07 ClimEcos (995) and EU-FP7-LUC4C (603542). The authors contributed equally to the conception of the work, design of the analysis, development of the methodology, and interpretation of results. R.A. was responsible for the data processing and artwork, and A.C. finalized the writing of the text.

SUPPLEMENTARY MATERIALS

www.sciencemag.org/content/351/6273/600/suppl/DC1
Materials and Methods
Supplementary Text
Figs. S1 to S11
Table S1
References (*28*–*39*)

17 June 2015; accepted 7 January 2016
10.1126/science.aac8083

CANCER THERAPEUTICS

Allele-specific inhibitors inactivate mutant KRAS G12C by a trapping mechanism

Piro Lito,[1]* Martha Solomon,[2] Lian-Sheng Li,[3] Rasmus Hansen,[3] Neal Rosen[1,2]*

It is thought that KRAS oncoproteins are constitutively active because their guanosine triphosphatase (GTPase) activity is disabled. Consequently, drugs targeting the inactive or guanosine 5′-diphosphate–bound conformation are not expected to be effective. We describe a mechanism that enables such drugs to inhibit KRAS^{G12C} signaling and cancer cell growth. Inhibition requires intact GTPase activity and occurs because drug-bound KRAS^{G12C} is insusceptible to nucleotide exchange factors and thus trapped in its inactive state. Indeed, mutants completely lacking GTPase activity and those promoting exchange reduced the potency of the drug. Suppressing nucleotide exchange activity downstream of various tyrosine kinases enhanced KRAS^{G12C} inhibition, whereas its potentiation had the opposite effect. These findings reveal that KRAS^{G12C} undergoes nucleotide cycling in cancer cells and provide a basis for developing effective therapies to treat KRAS^{G12C}-driven cancers.

Wild-type RAS guanosine triphosphatases (GTPases) cycle between an active, guanosine 5′-triphosphate (GTP)–bound, and an inactive, guanosine 5′-diphosphate (GDP)–bound, state (*1*, *2*). This is mediated by nucleotide exchange factors, which catalyze the exchange of GDP for GTP, and GTPase-activating proteins, which potentiate a weak intrinsic GTPase activity (*3*). Cancer-causing mutations impair the GTPase activity of RAS, causing it to accumulate in the activated state (*4*–*6*). Despite the prevalence of these mutations, no therapies that directly target this oncoprotein are currently available in the clinic (*7*–*9*). A recently identified binding pocket in KRAS^{G12C} (*10*) now enables the discovery of compounds that potently inhibit KRAS-GTP or effector signaling by this mutant.

[1]Department of Medicine, Memorial Sloan Kettering Cancer Center, New York, NY, USA. [2]Molecular Pharmacology Program, Memorial Sloan Kettering Cancer Center, New York, NY, USA. [3]Wellspring Biosciences, La Jolla, CA, USA.
*Corresponding author. E-mail: rosenn@mskcc.org (N.R.); litop@mskcc.org (P.L.)

Here we characterize a novel compound, ARS853, designed to bind KRAS^{G12C} with high affinity (*11*). The structures of ARS853 and previously reported (*10*) compounds (cmpds) 6 and 12 are shown in fig. S1A. Treatment of KRAS^{G12C}-mutant lung cancer cells with ARS853 reduced the level of GTP-bound KRAS by more than 95% (Fig. 1A, 10 μM). This caused decreased phosphorylation of CRAF, ERK (extracellular signal–regulated kinase), and AKT. In contrast, even at the highest concentration tested, cmpd 6 or 12 had only a minimal effect on pCRAF and pERK, without affecting KRAS-GTP levels (Fig. 1A and fig. S1B). ARS853 inhibited proliferation with an inhibitory concentration 50% (IC_{50}) of 2.5 μM, which was similar to its IC_{50} for target inhibition (Fig. 1, A and B). ARS853 (10 μM) inhibited effector signaling (Fig. 1C and fig. S1C) and cell proliferation (Fig. 1D and fig. S2) to varying degrees in six KRAS^{G12C} mutant lung cancer cell lines, but not in non-KRAS^{G12C} models (Fig. 1E and fig. S1, C and D). Similarly, it completely suppressed the effects of exogenous KRAS^{G12C} expression on KRAS-GTP levels, KRAS-BRAF interaction, and ERK signaling (fig. S1E). Inhibitor treatment also induced apoptosis in four KRAS^{G12C} mutant cell lines (Fig. 1, F to H). Thus, ARS853 selectively reduces KRAS-GTP levels and RAS-effector signaling in KRAS^{G12C}-mutant cells, while inhibiting their proliferation and inducing cell death.

In contrast to the rapid inhibition of signaling by kinase inhibitors, inhibition of KRAS^{G12C} by ARS853 occurred slowly (Fig. 2A and fig. S3). In some cell lines, maximal inhibition of KRAS-GTP occurred in 6 hours; in others, in 48 to 72 hours. To understand this phenomenon, we examined the mechanism of KRAS^{G12C} inhibition in more detail. To determine whether ARS853 binds to the active or the inactive conformation of KRAS^{G12C}, we used differential scanning fluorimetry, which assays ligand-induced changes in protein thermal stability (*12*). Recombinant KRAS^{G12C} was loaded with either GTPγS or GDP (fig. S4A) and then incubated with ARS853. Samples were incubated at increasing temperatures in the presence of a fluorescent dye that binds to hydrophobic surfaces exposed during thermal denaturation. ARS853 increased the amplitude of the thermal denaturation curve of KRAS^{G12C} loaded with GDP but not with GTPγS (Fig. 2B and fig. S4B). ARS853 did not alter the denaturation curve of GDP-loaded KRAS^{WT} (fig. S4C). These data suggest that ARS853 preferentially interacts with inactive, or GDP-bound, KRAS^{G12C}.

KRAS mutants are thought to exist in a "constitutively" active (GTP-bound) state in cancer cells (*13*). Thus, inhibition of KRAS-GTP levels by a drug that preferentially interacts with GDP-bound mutant KRAS is puzzling. Codon 12 mutations disable the activation of RAS GTPase by GTPase-activating proteins (*14*–*16*). It is possible, however, that the basal GTPase activity of KRAS^{G12C} is sufficient to enable nucleotide cycling in cancer cells. Consequently, we hypothesized that binding of the inhibitor to KRAS^{G12C} traps it in an inactive (GDP-bound) conformation by reducing its susceptibility to exchange, which then results in the observed time-dependent reduction in cellular KRAS-GTP levels. For this to be the case, (i) inhibition by the drug should require KRAS^{G12C} GTPase activity. (ii) If KRAS^{G12C} GTPase activity is constant, the rate of RAS inhibition by the drug should depend on exchange factor activity. (iii) Regulating exchange factor activity

Biophysical climate impacts of recent changes in global forest cover

Ramdane Alkama and Alessandro Cescatti

Science **351**, 600 (2016);
DOI: 10.1126/science.aac8083